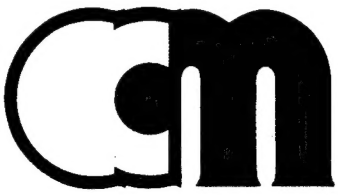

CCM-82-17

COMPRESSIVE STRENGTH OF COMPOSITE LAMINATES WITH INTERLAMINAR DEFECTS

JOHN W. GILLESPIE, JR.

R. BYRON PIPES

CENTER FOR COMPOSITE MATERIALS

College of Engineering
University of Delaware
Newark, Delaware

COMPRESSIVE STRENGTH OF COMPOSITE LAMINATES WITH INTERLAMINAR DEFECTS

John W. Gillespie, Jr.

R. Byron Pipes

Center for Composite Materials
University of Delaware
Newark, Delaware

Sponsored by the

University-Industry Research Program
"Application of Composite Materials
to Industrial Products"

September 1982

ABSTRACT

The compressive strength of composite laminates is greatly reduced by the local instabilities initiated by interlaminar defects. In the present study, the reduction in compressive strength of a $(0/\pm45_2/0)s$ AS/3501-6 graphite-epoxy laminate containing implanted interlaminar defects is examined. The experimental study consisted of the four-point static loading of sandwich beams with graphite-epoxy face sheets having through-width delaminations of 0.5 in. (12.7mm), 0.75 in. (19.1mm), 1.0 in. (25.4mm) and 1.5 in. (38.1mm) in length. Failure consisted of the unstable interlaminar crack growth within the compressive face of the sandwich. Reduction in flexure strength was found to be directly proportional to debond length and varied from 41 to 87 percent of the pristine value. Combined stability and finite element analysis showed that the initial out-of-plane deformations of the sublaminate induced by residual stresses decreases axial stiffness of the buckled sublaminate and results in both Mode I and Mode II propagation at the interlaminar crack tip. An approximate strain energy release rate formulation for Mode I fracture is correlated with the experimental data, where a value of the strain energy

release rate G_{IC} = 1.4 lb/in (250N/m) yields accurate predictions of the compressive strength for all defect geometries considered.

INTRODUCTION

The local instability of composite laminates in the vicinity of interlaminar defects may strongly influence the compressive strength of the laminate. In an attempt to quantify this phenomenon, composite sandwich beams with implanted interlaminar defects of PTFE film were tested in four point flexural loading. Experimental results showed substantial reductions in strength with increasing defect length.

Failure occurred on the compressive face of the sandwich beam for all specimens including the zero defect geometry. The failure mechanism consisted of fast interlaminar fracture initiating at the interlaminar crack tip [1]. Reduction in the flexure strength varied from 41 to 87 percent of the zero defect value for the debond lengths investigated. The drastic reduction in strength is attributed to the decrease in stiffness of the buckled sublaminate. Consequently, additional load is transferred through shear at the edge of the defect to the sublaminate which remains bonded to the honeycomb core and is thus restrained from buckling.

The complex state of stress at the crack-tip

resulting from the reduction is stiffness, as well as, the curvature of the buckled sublaminate arising from out-of-plane deformations has been investigated by Gillespie and Pipes [2] and Whitcomb [3] using linear and non-linear finite element techniques, respectively. The interlaminar normal and shear stress components exhibit singular behavior at the crack tip suggesting the total strain energy release rate has contributions from both Mode I and Mode II crack extension modes. Ashizawa [1] and Whitcomb [3], however, have shown that delamination growth may be dominated by Mode I fracture.

In the present analysis of the sandwich beam the slight variation of compressive stress (approximately 4 percent) across the laminate thickness and the sandwich beam curvature are neglected. The debond region is modeled as two beams in parallel, one straight and one which exhibits lateral deformation and thus reduced axial stiffness. Compatability of axial displacements at the end of the beam model enables the total axial load to be divided between the two beams in direct proportion to their apparent stiffnesses. Initial out-of-plane deformation of the sublaminate above the defect due to the debond thickness* and thermal residual stresses is included in the buckling analysis and

---

(*The debond was produced by implanting a 0.002 in (0.05mm) PTFE insert.)

significantly reduces the axial stiffness of the deformed sublaminate. Employing this model to predict the axial load at failure in the deformed laminate results in loads substantially less than the classical Euler's buckling load for the majority of delaminations investigated [1]. Consequently, the post-buckling analyses of Chai [4] and Whitcomb [5] may not be applicable for delaminations of sublaminates with initial deflections.

The strain-energy release rate for a cantilever beam loaded by a moment is employed to correlate experimental failure loads with analytic predictions. The eccentricity in the load path where the axial load is transferred through interlaminar stresses in the vicinity of the crack tip results in a crack closing moment whose magnitude is directly proportional to the reduction in axial stiffness of the buckled sublaminate. Linear finite-element stress analysis of the crack tip region is employed by replacing the nonlinearity of the buckled sublaminate with an equivalent set of loads determined from the beam model. Finite element results reveal that the interlaminar state of stress is a boundary layer phenomenon and thus independent of debond length. The boundary layer of interlaminar stresses is analogous to that described in the free-edge problem [6] and is equal to three laminate thicknesses for the laminate geometries considered. The closing moment results from the

interlaminar normal stress distribution at the crack tip and the magnitude is evaluated through numerical integration techniques or through equilibrium considerations of an appropriate free-body diagram of the delamination region. Consequently, the total moment in the strain energy release rate formulation is the summation of the opening and closing moments acting at the crack tip [5]. A value of G_{IC} = 1.4 lb/in (250 N/m) yields accurate predictions of the compressive strength for the delamination geometries considered.

EXPERIMENTAL EFFORT

The experimental effort consisted of the four-point static loading of sandwich beams with $[0/\pm45_2/0]_s$ AS/3501-6 graphite-epoxy face sheets (Figure 1). Implanted through-width delaminations of 0.5 in. (12.7mm), 0.75 in. (19.1mm), 1.0 in. (25.4mm) and 1.5 in. (38.1mm) in length were placed at the midsurface between the zero degree plies and co-cured with the laminate. The implanted defects consisted of two rectangular layers of 0.001 in. (0.0254mm) PTFE film and represents the minimum initial out-of-plane deformation of the sublaminate as shown schematically in Figure 1.

Experimental results presented in Table 1 show the equivalent flexure stress and strain in the compressive face sheet at failure. Instrumentation consisted of strain gages centered directly over the implanted defects on both the tensile and compressive faces of the sandwich beam. The strain on the compressive face consisted of contributions from the curvature of the buckled sublaminate, as well as, the axial loading. Consequently, any appreciable buckling would reduce the compressive strain (ε_c) relative to the strain on the tensile face (ε_T). The characteristic strain responses (ε_T vs ε_c) are illustrated in Figure 2 for the

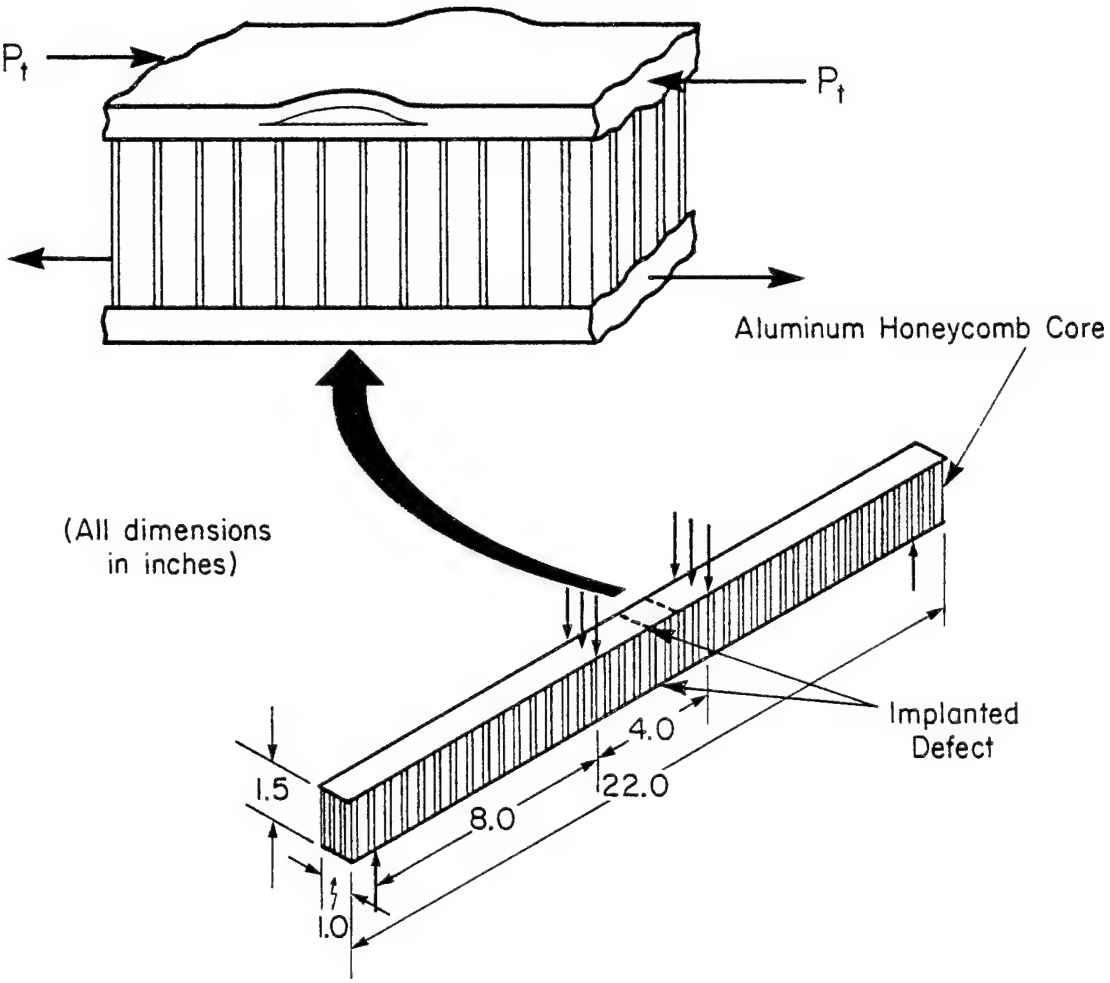

Figure 1. Test Specimen

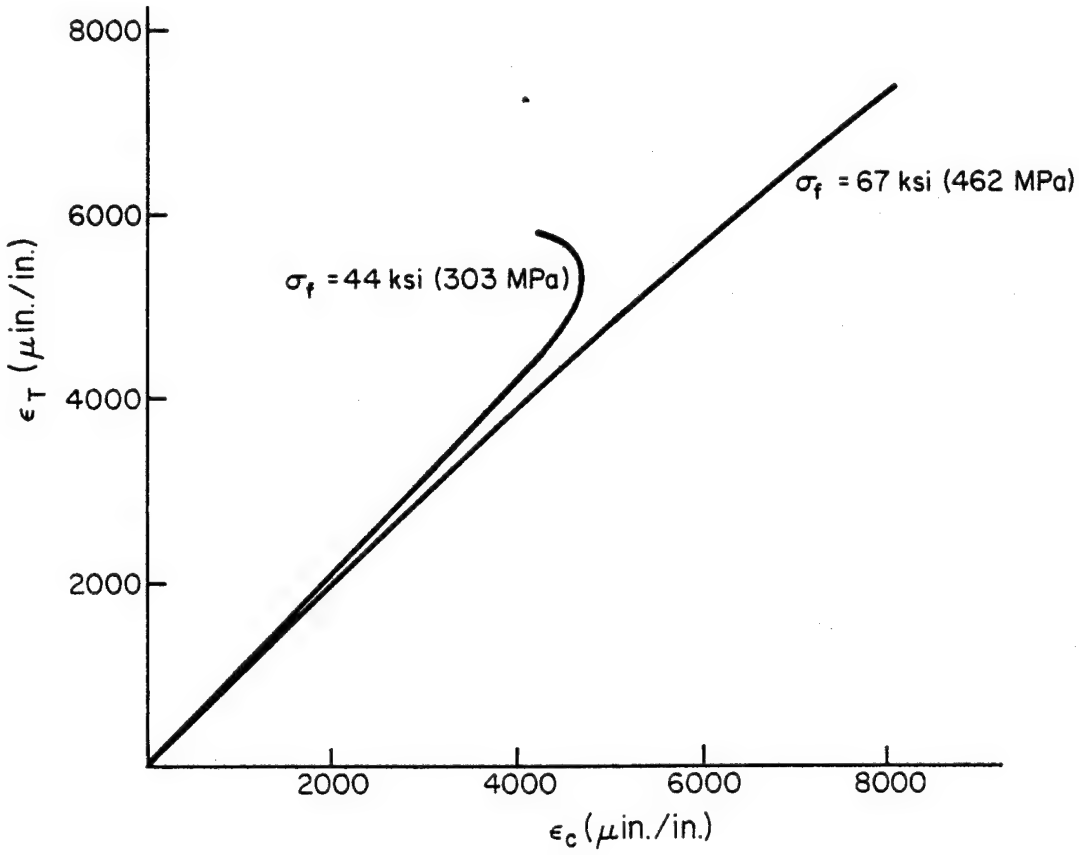

Figure 2. Strain Response for the 0.75 in. (19.1 mm) Sandwich Beam

0.75 in. (19.1mm) defect which exhibits a transition from the linear to nonlinear response prior to failure.

Table 1

Experimental Data*

Debond length inches (mm)	Failure Stress Ksi (MPa)	Compressive Failure Strain με
0	102.0 (703)	14500
0.50** (12.7)	58.8 (411)	7250
0.75 (19.1)	55.6 (383)	6625
1.00 (25.4)	25.9 (179)	3000
1.50 (38.1)	13.4 (92)	1300

* Minimum of four tests/geometry
** Two tests only

In Figure 3, the reduction in strength with increasing debond length illustrates the strong dependence of compressive strength on interlaminar defect geometry. The characteristic failure mode for sandwich beams with implanted defects was fast interlaminar fracture at the mid-surface of the compressive face sheet as shown in Figure 4. Crack arrestment occurred at the load introduction points of the fixture.

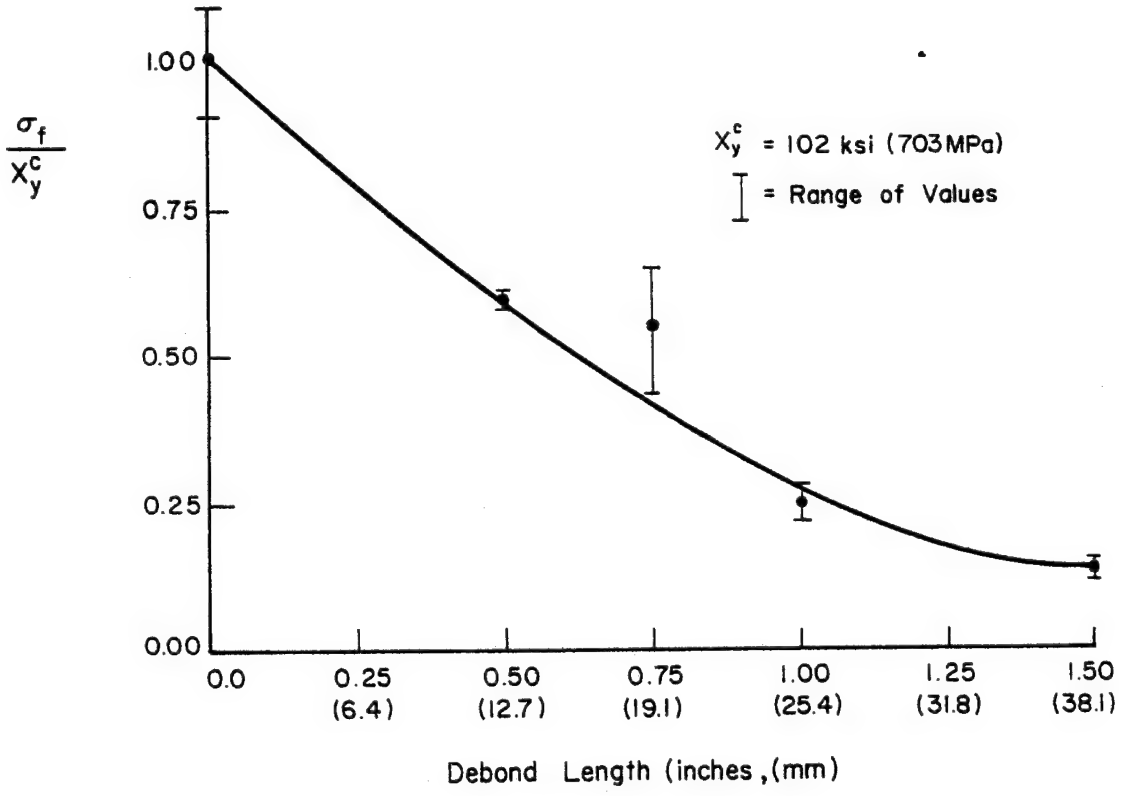

Figure 3. Reduction in Strength as a Function of Debond Length

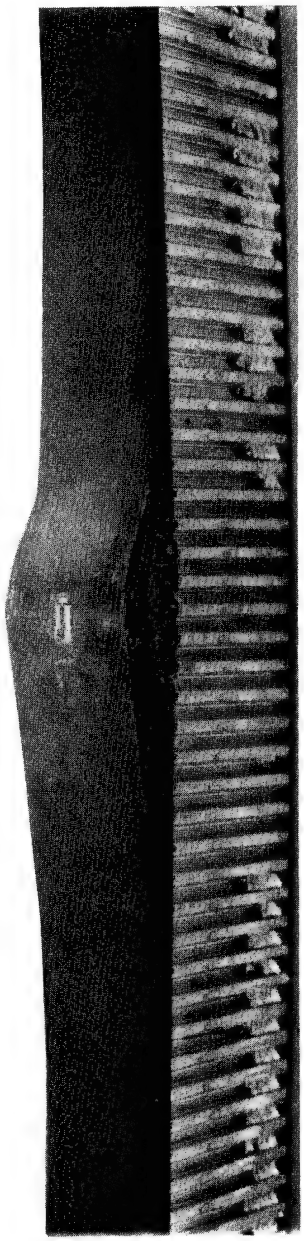

Figure 4. Characteristic Failure Mode

STRESS ANALYSIS

Investigation of the complex state of stress in the vicinity of the crack tip due to the reduction in axial stiffness of the buckled sublaminate necessitated finite element analysis. In general, a geometrically non-linear finite element stress analysis would be required [3]. In the present study, however, linear finite element stress analysis of the crack tip region is employed by replacing the non-linearity of the buckled sublaminate with an equivalent set of loads determined from the beam model. The finite element model is shown in Figure 5 where the buckled sublaminate is replaced by equivalent forces. Mesh refinement in the vicinity of the defect is required due to the presence of large stress gradients. Symmetry enabled one-half of the debond region to be modelled. The total length of the model was 2 in. (50.8mm) or one-half the distance between the beam load introduction points. The length of the step was one-half the debond size. The boundary conditions are indicated clearly in Figure 5.

The lamina properties for unidirectional AS/3501-6 graphite-epoxy are presented in Table II. The effective properties for the $(0/\pm45_2/0)_s$ laminate employed in the

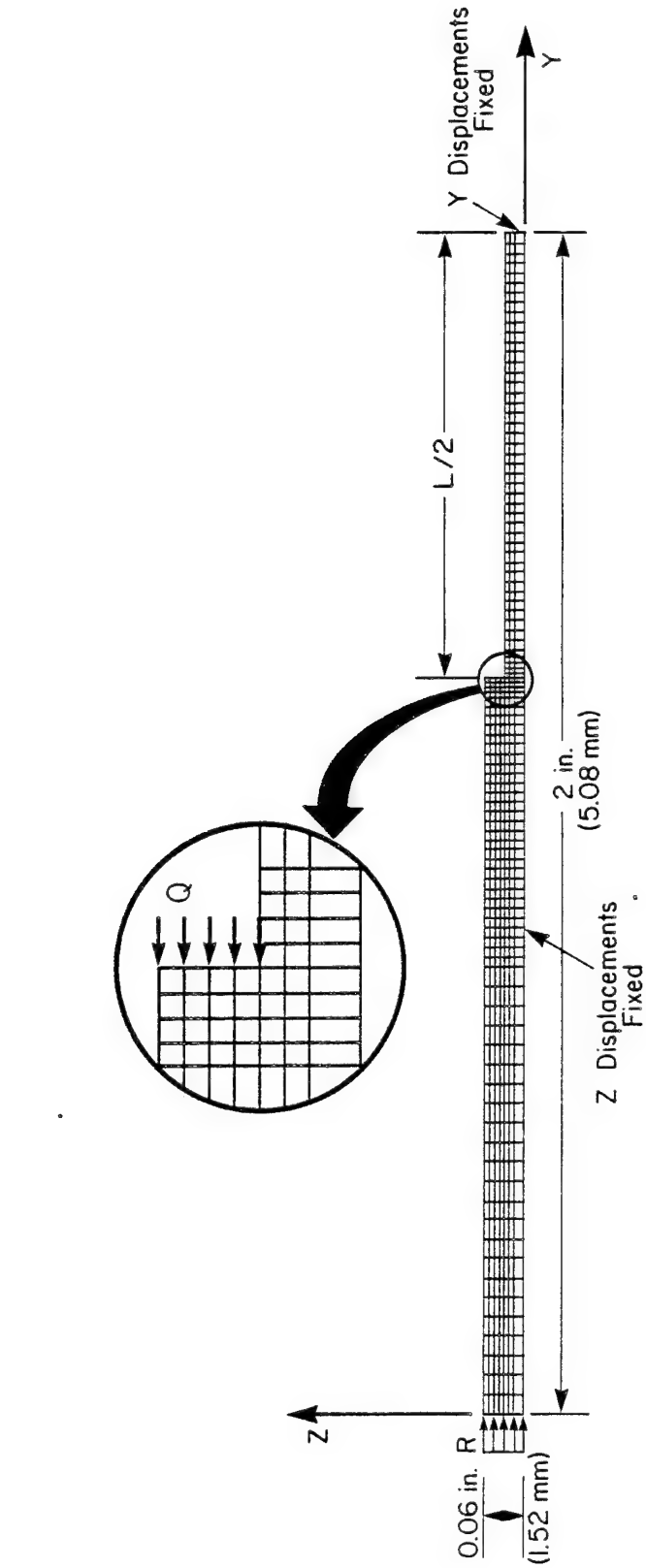

Figure 5. Finite Element Model of the Defect Region on the Compression Face

Table II

Laminar Properties: AS/3501-6

E_1 Msi (GPa)	19.9	(137.2)
E_2 Msi (GPa)	1.4	(9.7)
E_3 Msi (GPa)	1.4	(9.7)
ν_{12}	0.21	
$\nu_{13} = \nu_{12}$	0.21	
ν_{23}	0.3	
G_{12} Msi	0.6	(4.1)
$G_{13} = G_{23} = G_{12}$ Msi (GPa)	0.6	(4.1)

Table III

Effective Laminate Properties: $[0/\pm 45_2/0]_s^*$

E_y Msi (GPa)	8.2	(56.5)
E_x Msi (GPa)	3.5	(24.1)
E_z Msi (GPa)	1.4	(9.7)
ν_{yx}	0.74	
ν_{yz}	0.067	
ν_{xz}	0.215	
G_{xy} Msi (GPa)	3.7	(25.5)
$G_{xz} = G_{yz} = G_{xy}$ Msi (GPa)	3.7	(25.5)

* 0° plies are parallel to beam axis

finite element model are given in Table III.

The loadings considered are defined in Figure 5 and consist of the applied axial stress (R) and the equivalent axial stress (Q) applied at the end of the defect. Since a linear solution is obtained, each loading is investigated separately and the total solution is obtained by a superposition of results. The stress components along the fracture surface have apparent singularties at the crack tip which diminish within three laminate thicknesses to a uniform state of stress. The finite element analysis of various defect lengths indicate no dependence of the stress distribution on debond length. Consequently, a single finite element model in conjunction with the buckling analysis is sufficient to characterize the stress state in the vicinity of the interlaminar crack and represents a major simplification of the non-linear problem.

In Figure 6, the distributions of the axial stress component σ_y for the axial stress tractions R and Q are presented. Note the localized variation of stress which diminishes rapidly to a uniform state of stress at y/h = -3. An axial stress R of unit magnitude applied to the model remains constant (equal to -1), attains a maximum at the crack tip and decays to twice the applied stress as required by equilibrium.

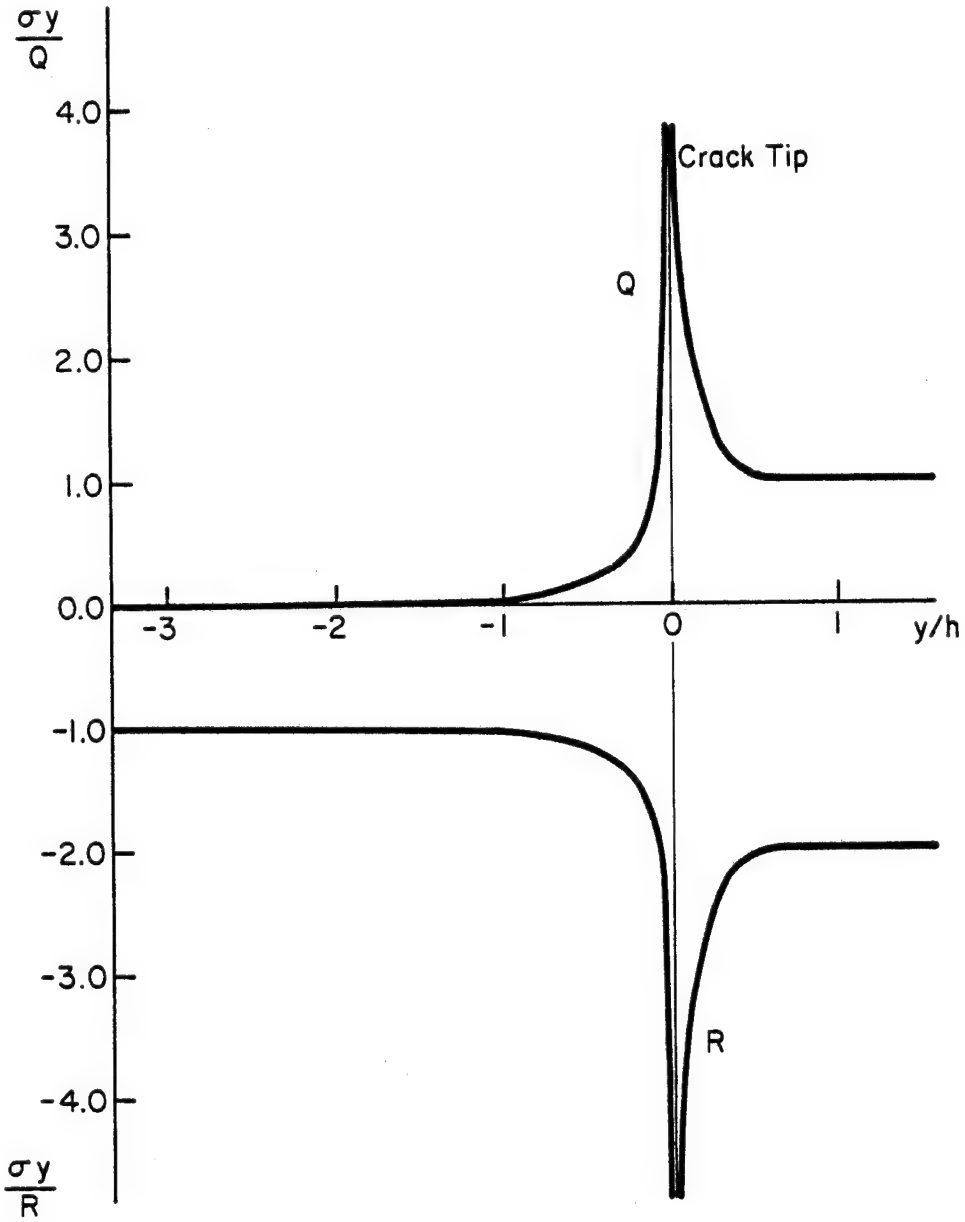

Figure 6. Axial Stress Distribution Along Section A-A: Axial Loading

In Figure 7 and 8, the interlaminar shear and normal stress distributions are presented. All profiles are symmetric with respect to stress tractions R and Q and appear singular at the crack tip. Consequently, the interlaminar state of stress exists only for sublaminate geometries having reduced axial stiffness ($Q<R$) as determined in the flexural analysis. The interlaminar shear stress distribution presented in Figure 7, represents the axial load transferred to the sublaminate bonded to the honeycomb core and restrained from buckling. The eccentricity in the load path, however, establishes the interlaminar normal stress distribution at the crack tip shown in Figure 8. Note that the regions of tensile and compressive stresses are equal in area as required by equilibrium. For $Q<R$, the interlaminar normal stress distribution generates a crack closing moment which will be included in the strain-energy release rate formulation for the prediction of compressive strength of composite laminates with interlaminar defects.

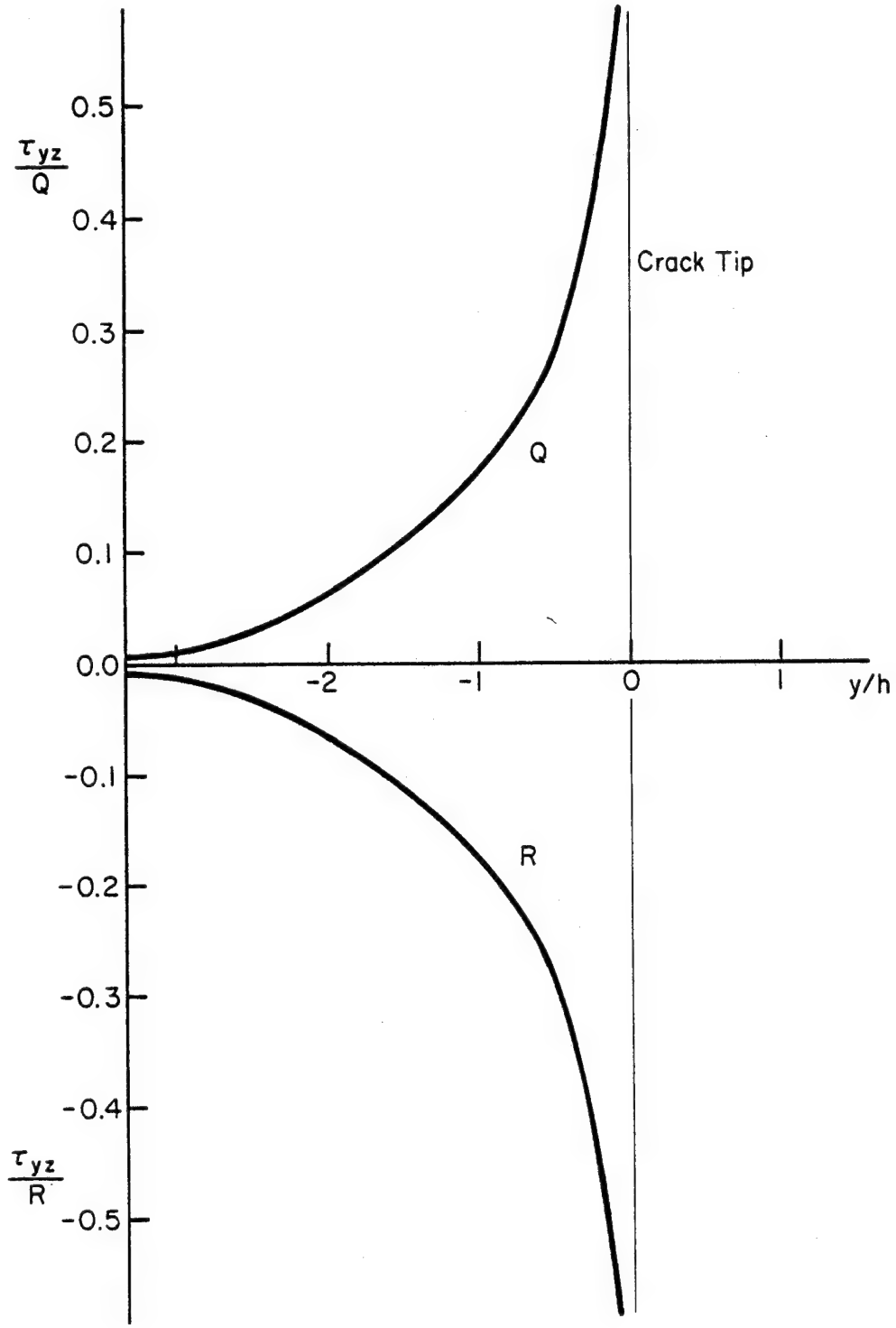

Figure 7. Shear Stress Distribution Along Section A-A: Axial Loading

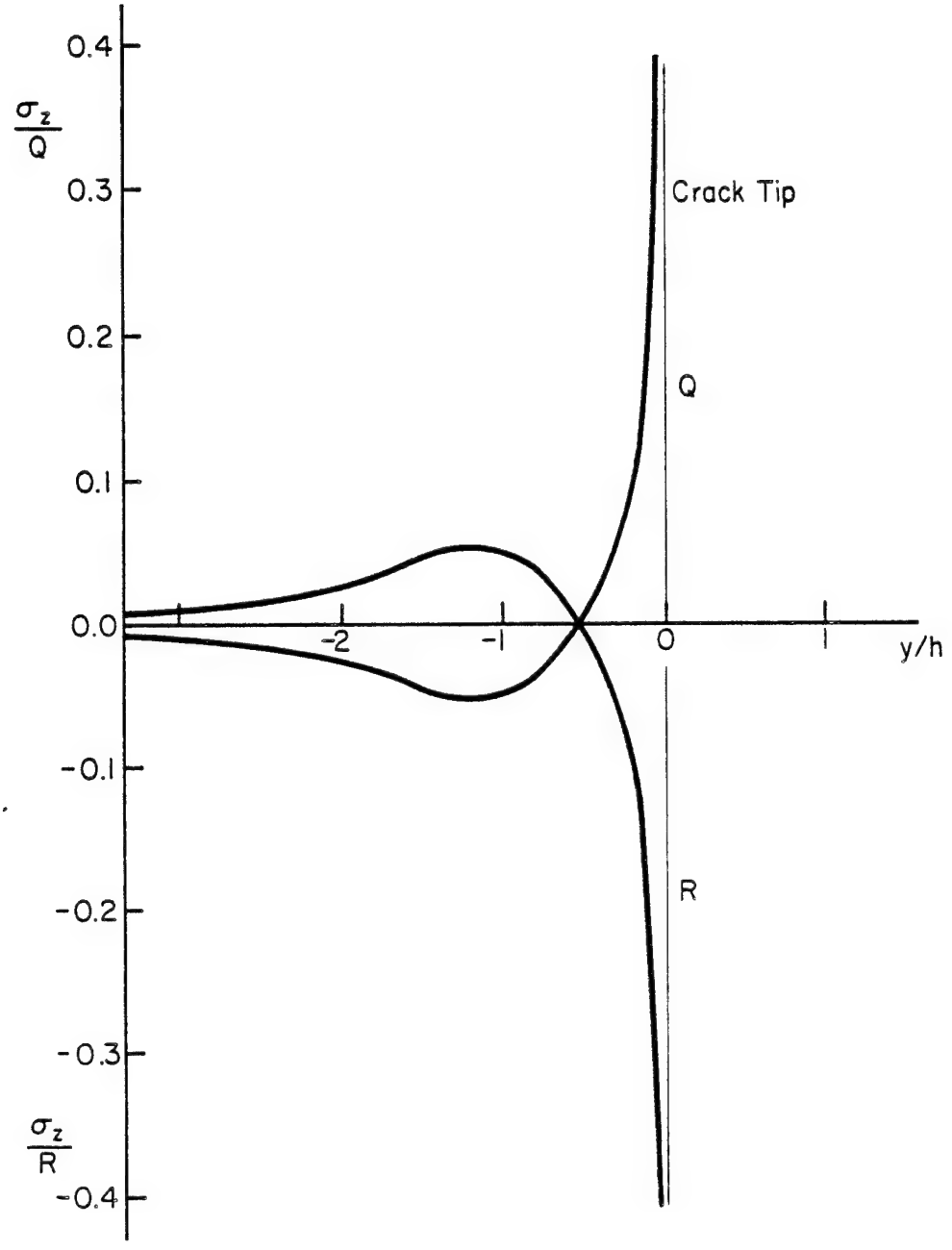

Figure 8. Interlaminar Normal Stress Distribution Along Section A-A: Axial Loading

FLEXURAL INSTABILITY OF COLUMNS

The slight variation of flexure stress across the laminate thickness and the sandwich beam curvature are neglected. The debond region is modelled as two beams in parallel, one straight and one which exhibits lateral deformations. Consider a uniform contraction, Δ, of the beam model shown in Figure 9. The loads carried by the two beams are proportional to their stiffness:

$$P_t = P_s + P_b = \left(\frac{A_s E_s}{L} + K_b\right)\Delta \qquad (1)$$

where K_b is the stiffness of the buckled beam determined from the flexural analysis presented below. Therefore, for a specified initial imperfection, one interates on the axial displacement until the total axial loads equals the experimental value at failure. The loadings in the buckled subliminate can then be substituted into the stress analysis (Figures 6-8) to determine specific distributions for the various stress components. The stress tractions, R and Q, are simply the appropriate axial loads divided by the cross-sectional area of the sublaminate.

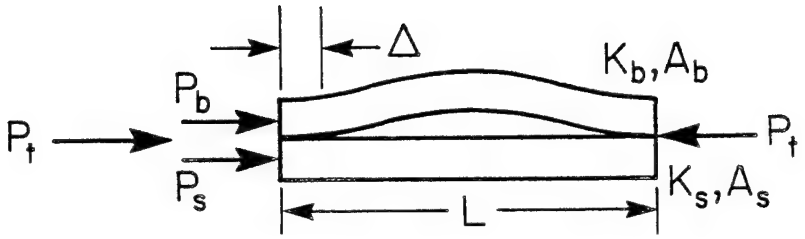

$$P_t = P_s + P_b$$

$$= (K_s + K_b)\Delta$$

where $$K_s = \frac{A_s E_s}{L}$$

$$K_b = K_b(L, W, P_b)$$

Figure 9. Beam Model

Consider the axially loaded beam with arbitrary initial deformation $w_o(y)$ shown in Figure 10. The governing differential equation in terms of the bending deformation, $w_1(y)$ measured from the initial shape, is given by

$$\frac{d^2}{dy^2}(E_b I_b \frac{d^2 w_1}{dy^2}) - \frac{d}{dy}(N \frac{d(w_1+w_o)}{dy} = 0 \qquad 0 \leq y \leq L \tag{2}$$

$$\frac{dN}{dy} = \frac{d}{dy}[E_b A_b (\frac{du}{dy} + 1/2(\frac{dw_1}{dy})^2] = 0 \tag{3}$$

where N = axial forces

E_b = effective laminate modulus

u = axial displacement

w_1 = lateral bending deformation

A_b = cross sectional area

I_b = moment of inertia

The boundary conditions for the clamped-clamped beam subjected to an axial displacement, Δ are:

$$w_1(0) = 0 \qquad w_1(L) = 0 \tag{4}$$

$$\frac{dw_1}{dy}(0) = 0 \qquad \frac{dw_1}{dy}(L) = 0 \tag{5}$$

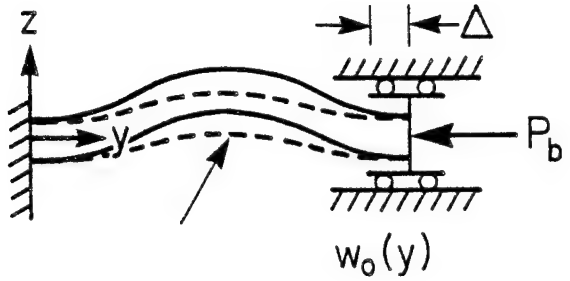

$$w_o(y) = \frac{W}{2}\left(1 - \cos\left(\frac{2\pi y}{L}\right)\right)$$

$$w(y) = \frac{2\pi^2 W\left(1 - \cos\left(\frac{2\pi y}{L}\right)\right)}{4\pi^2 - (\lambda L)^2}$$

$$\Delta = \frac{P_b L}{E_b A_b} + \frac{\pi^2 (\lambda L)^4 W^2}{4L\left(4\pi^2 - (\lambda L)^2\right)^2}$$

$$M_b = \frac{W}{L^2}\left(\frac{8\pi^4 E_b I_b}{4\pi^2 - (\lambda L)^2}\right)$$

$$\lambda = \sqrt{P_b / E_b I_b}$$

Figure 10. Initially Deformed Beam - Column

$$u(0) = 0 \qquad u(L) = -\Delta \tag{6}$$

The solution of Equation (3) implies that the axial force in the buckled laminate, N is a constant equal to:

$$N \equiv -P_b = E_b A_b \left(\frac{du}{dy} + \frac{1}{2}\left(\frac{dw_1}{dy}\right)^2\right) \tag{7}$$

For $E_b I_b$ constant, Equation (2) simplifies to the following

$$\frac{dw_1^4}{dy^4} + \lambda^2 \frac{d^2 w_1}{dy^2} = -\lambda^2 \frac{d^2 w_o}{dy^2} \tag{8}$$

where

$$\lambda^2 = P_b / E_b I_b \tag{9}$$

In the following analysis, $w_o(y)$ is assumed to be the first eigenvector of the clamped-clamped beam,

$$w_o(y) = \frac{W}{2}\{1-\cos \frac{2\pi y}{L}\} \tag{10}$$

where W is the maximum deflection at the center of the beam. Substitution of Equation (10) into Equation (8) yields

$$\frac{d^4w_1}{dy^4} + \lambda^2 \frac{d^2w_1}{dy^2} = - \frac{\lambda^2 2W\pi^2}{L^2} \cos \frac{2\pi y}{L} \tag{11}$$

The general solution of equation (11) is

$$w_1(y) = C_1 \cos \lambda y + C_2 \sin \lambda y + C_4 + w_{1p}(y) \tag{12}$$

where $w_{1p}(y)$ is the particular solution given by

$$w_{1p}(y) = \frac{-\lambda^2 W \cos \frac{2\pi y}{L}}{2(\frac{4\pi^2}{L^2} - \lambda^2)} \tag{13}$$

Employing the boundary conditions in Equations (4) and (5) to determine the unknown constants yields

$$C_1 = C_2 = C_3 = 0$$

$$C_4 = \frac{\lambda^2 W}{2(\frac{4\pi^2}{L^2} - \lambda^2)} \tag{14}$$

The solution reduces to:

$$w_1(y) = \frac{(\lambda L)^2 W(1-\cos \frac{2\pi y}{L})}{2(4\pi^2-(\lambda L)^2)} \tag{15}$$

Performing the integration indicated in Equation (3) yields the following expression for the axial displacement,

$$\Delta = \frac{P_b L}{EA_b} + \frac{\pi^2 (\lambda L)^4 W^2}{4L(4\pi^2 - (\lambda L)^2)^2} \tag{16}$$

The total bending deformation is therefore:

$$w(y) = w_o(y) + w_1(y) = \frac{2\pi^2 W(1-\cos \frac{2\pi y}{L})}{(4\pi^2 - (\lambda L)^2)} \tag{17}$$

In the limit as the axial load tends to zero ($\lambda \to 0$), Δ tends to zero and the total bending deformation approaches the prescribed initial deflection $w_o(y)$. The solutions, however, share the common singularity at the Euler buckling load (P_{CR}).

In Figure 11, the axial load-displacement response of an initially deformed beam is presented. The axial load at which significant non-linear response initiates is inversely proportional to the initial deflection, W. With respect to the beam model in Figure 9, commencement of non-linear behavior corresponds to reduced axial stiffness of the buckled sublaminate and the transfer of load at the crack tip through interlaminar stresses to the sublaminate bonded to the honeycomb core (See Figure 10). Within the constraints of small deflection theory, the maximum

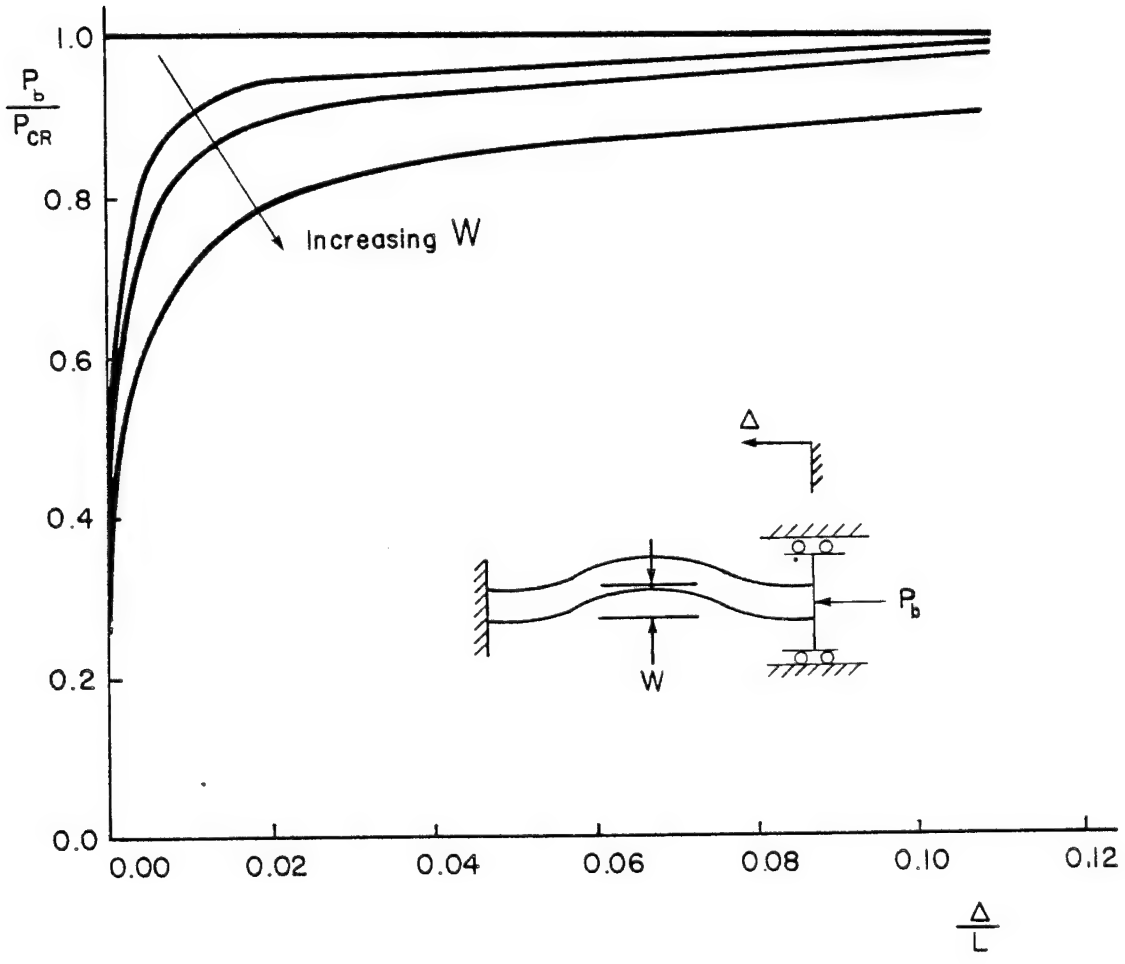

Figure 11. Axial Load-Displacement Response of an Initially Deformed Beam

axial load of an initially deformed beam at which point the axial stiffness tends to zero decreases with increasing W and is significantly less than the Euler buckling load assumed in the post-buckling analysis of Whitcomb [5] and Chai [4]. This phenomenon is clearly illustrated in Figure 12 where the stress component, Q, in the initially deformed sublaminate approaches the asymptote with increasing applied stress, R. Consequently, the stress component, S, in the sublaminate restrained from buckling is a monotonically increasing function of R as required by equilibrium. In Figure 13, the deleterious effects of the initial deflection, W, on the axial load-midspan deflection response is presented. For a prescribed axial loading, the bending deformations, as well as, the bending moment which initiates the Mode I crack propagation are directly proportional to the initial deflection W. Therefore, the compressive strength of composite laminates with interlaminar defects is inversely proportional to the magnitude of the initial out-of-plane deformations.

CORRELATION OF RESULTS

Correlation of experimental data with analytic predictions was based upon a strain-energy release rate formulation consistent with the approximations of simple beam theory. Whitcomb [3] and Ashizawa [1] have shown that Mode I strain energy release rate, G_I , dominates instability-related delamination growth. Consequently, the

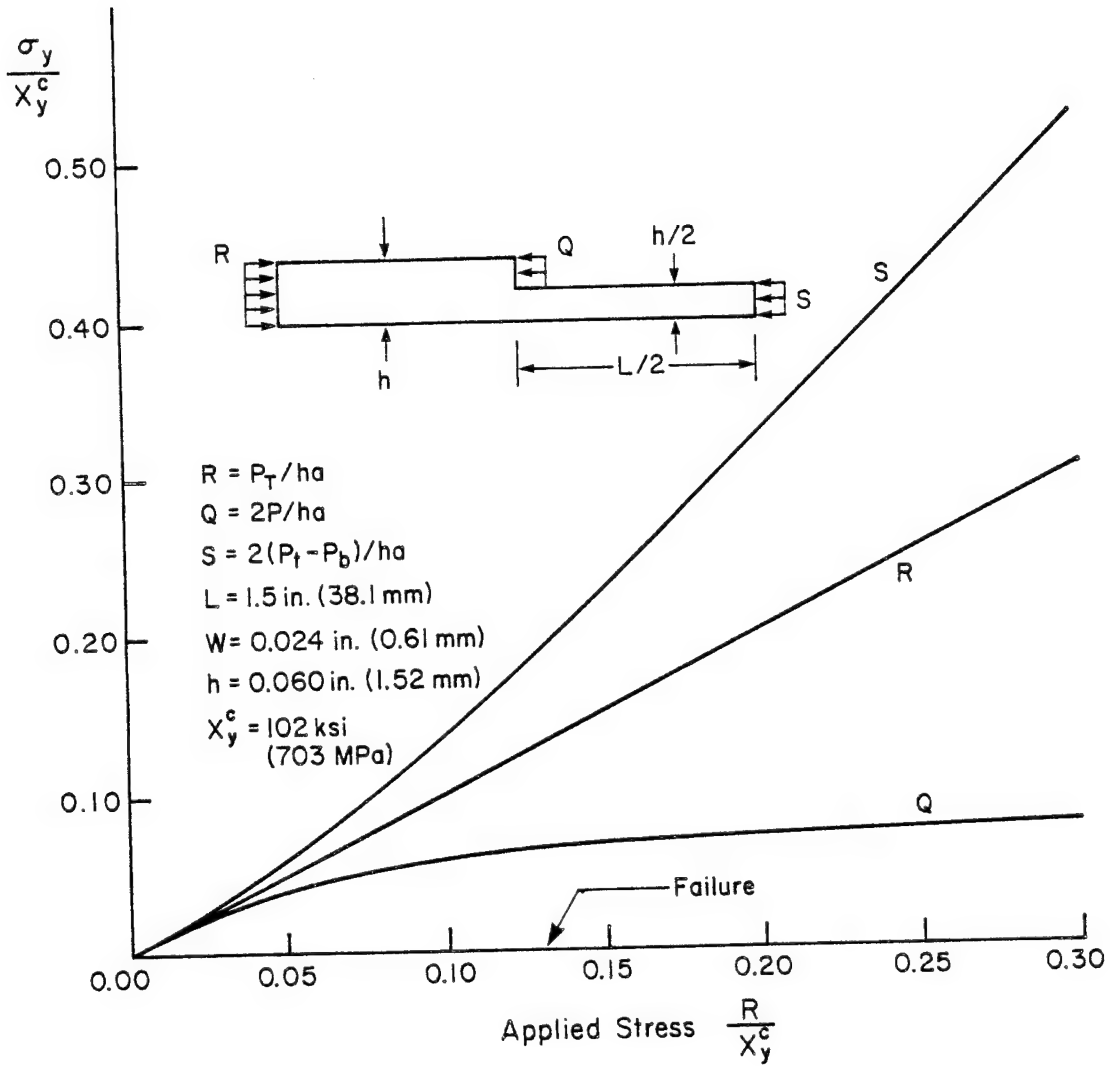

Figure 12. Influence of Applied Stress on Stress Resultants in Beam Model

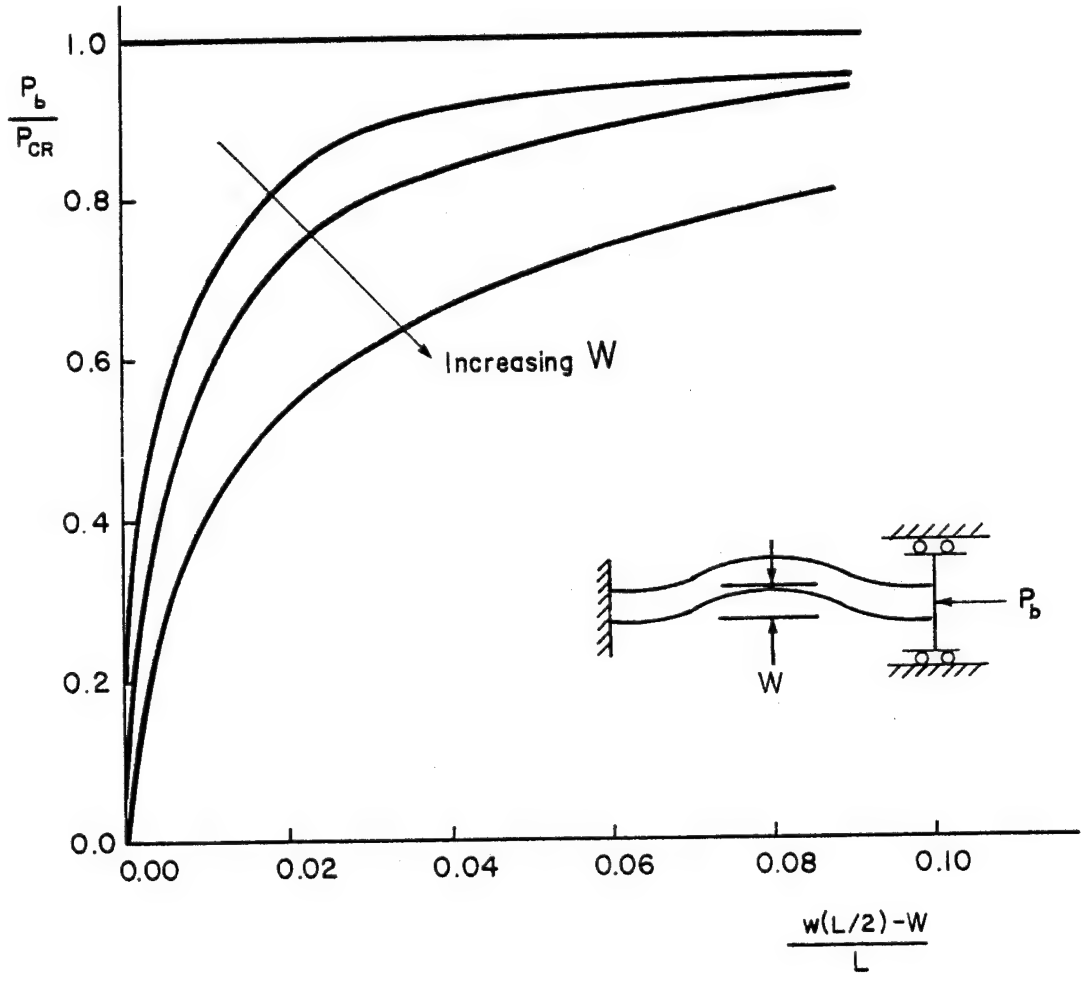

Figure 13. Axial Load-Midspan Deflection Response of an Initially Deformed Beam

Mode II contribution to the total strain-energy release rate will not be included in the present analysis.

The strain-energy release rate for a cantilever beam loaded by a moment is $M_T^2/2E_bI_ba$ [7] where M_T is the total applied moment at the crack tip and a is the width of the test specimen. As discussed previously, M_T represents the summation of the crack opening moment, M_b , and the crack closing moment, M_c ,

$$G_I = \frac{(M_b+M_c)^2}{2E_bI_ba} \tag{18}$$

The crack opening moment is obtained directly from the flexural analysis and successive differentiation of (17) yields,

$$M_b = \frac{W}{L^2}\left[\frac{8\pi^4E_bI_b}{4\pi^2-(\lambda L)^2}\right] \tag{19}$$

The crack closing moment arises from the reduced axial stiffness of the delamination and the eccentricity in the load path at the crack tip. An expression for M_c can be derived from the free body diagram in Figure 14.

Force summation in the "y" direction yields the shear force resultant τ, where

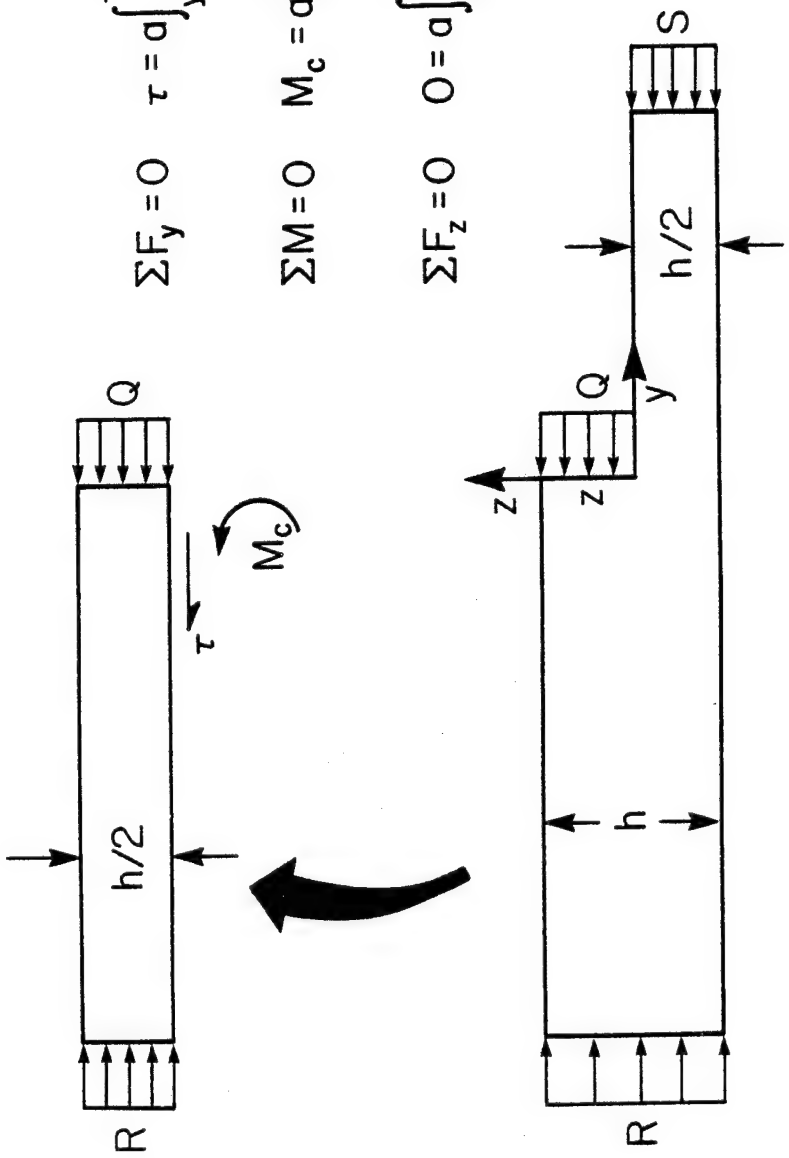

Figure 14. Free Body Diagram of Crack Front

$$\tau = a \int_{0}^{-3h} \tau_{yz}\, dy = (R-Q)\frac{ah}{2} \qquad (20)$$

The shear resultant, however, is not co-linear with the axial stress resultants and the moment M_c is produced at the crack tip. Summing moments yields the desired expression for the crack closing moment,

$$M_c = \frac{-a(R-Q)h^2}{8} \qquad (21)$$

The closing moment, however, corresponds to the moment associated with the interlaminar normal stress distribution presented in Figure 8. Numerical integration yields,

$$M_c = a \int_{0}^{-3h} \sigma_z\, ydy \approx \frac{-a(R-Q)h^2}{9.4} \qquad (22)$$

Further mesh refinement would reduce the discrepancy between equations (21) and (22) by providing improved approximation to the large stress gradients which exist in the vicinity of the crack tip. Additional finite element analysis is not required however since equation (21) is exact. The influence of applied loading on the moment resultant is presented in Figure 15 for a delamination length of 1.5 inches (38.1mm). Moments M_B and M_c are monotonically increasing

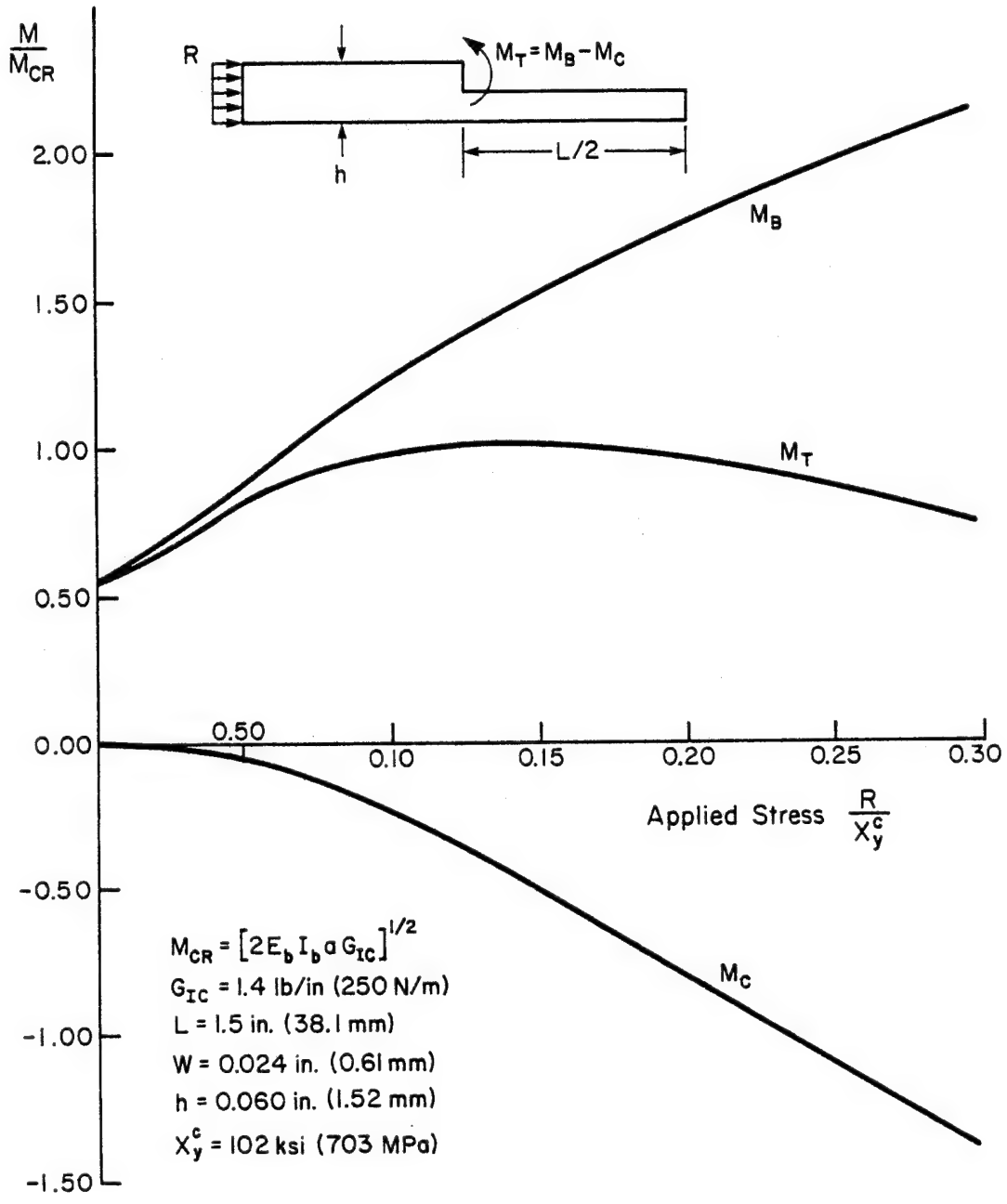

Figure 15. Influence of Applied Stress on Opening and Closing Moments

and decreasing functions of the applied load, respectively. The total moment, however, attains a global maximum through the interaction of the opening and closing moments of opposite sign. Employing equation (18), strain-energy release rate is presented as a function of the applied loading and several values of initial imperfections, W. The strain-energy release rate also exhibits maxima whose magnitude are directly proportional to the initial deflection, W. Interestingly, results presented in Figure 16 reveal the existence of stable configurations for which the available strain energy for delamination growth does not exceed the critical value (G_{IC}). In Figure 17, the non-dimensionalized strain-energy release rate (G/G_{IC}) as a function of applied load for the specific delamination length/initial deflection geometries encountered in the experiment effort is presented. Fast interlaminar fracture occurs when the strain-energy release rate equals the critical value as illustrated in Figure 17. A value of G_{IC} = 1.4 lb/in (250N/m) provides excellent correlation of experimental data with analytical predictions of the compressive strength of composite laminate with interlaminar defects (Figure 18).

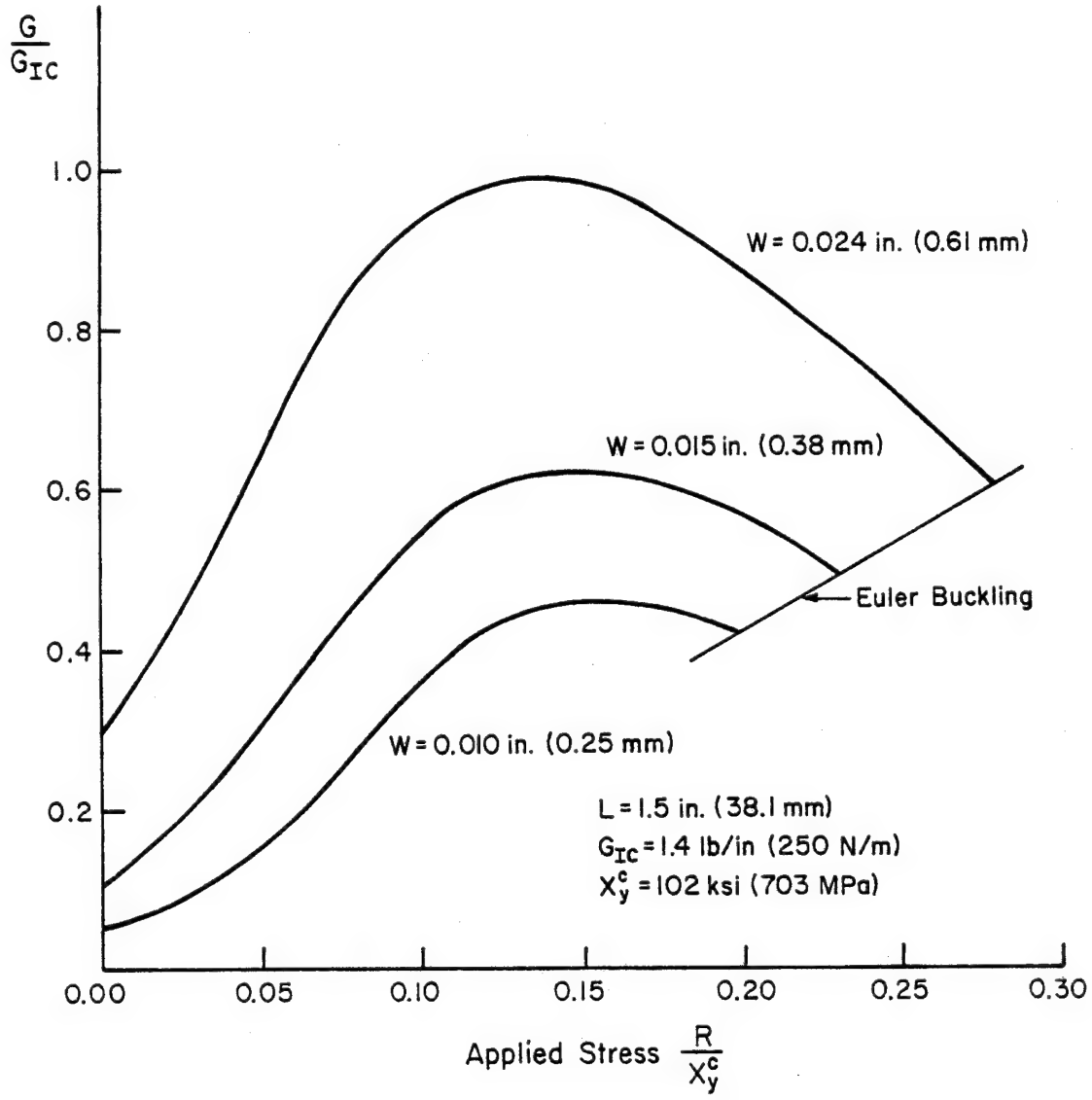

Figure 16. Strain Energy Release Rate as a Function of Initial Deflection (W)

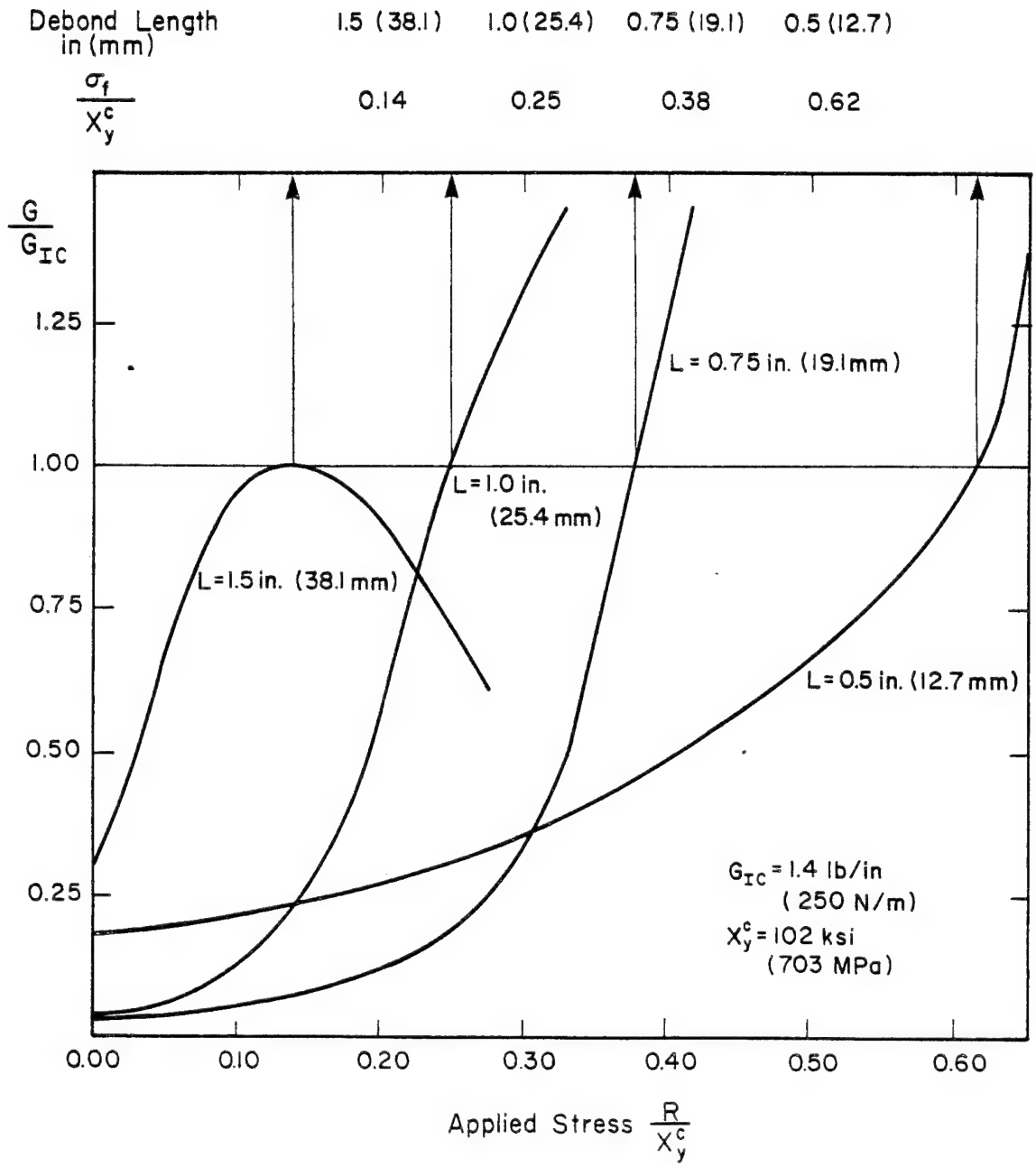

Figure 17. Compressive Strength Prediction

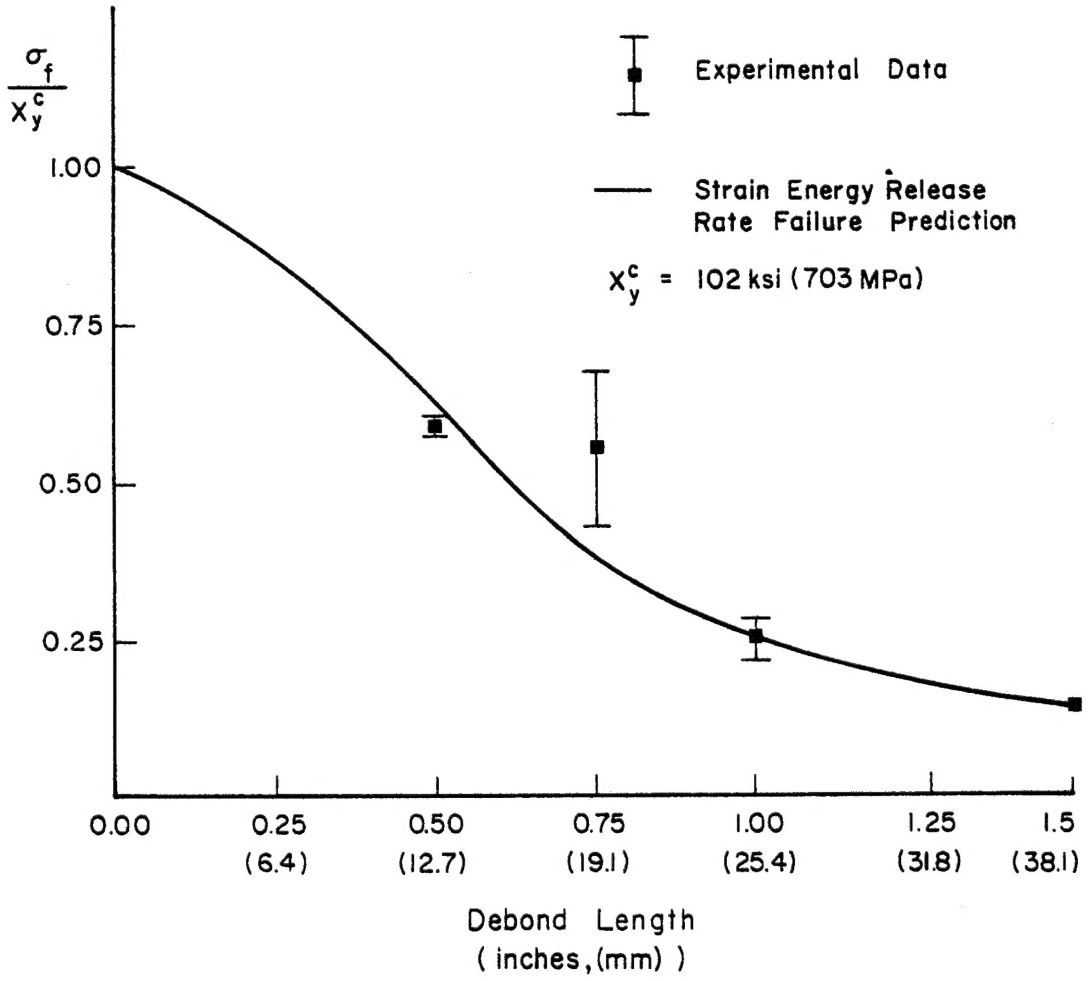

Figure 18. Correlation of Strain Energy Release Rate Failure Prediction with Experimental Data

CONCLUSIONS

The local instability of sublaminates due to interlaminar defects results in the drastic reduction in compressive strength of the laminate investigated. The presence of initial deformations results in reduced axial stiffness of the sublaminate for axial failure loads significantly less than the classical Euler's buckling load. Consequently, post-buckling analyses may not be applicable for delaminations with initial deflections. Linear finite element stress analysis of the crack tip region is employed by replacing the non-linearity of the initially deformed sublaminate with an equivalent set of loads determined from the beam model. The interlaminar state of stress diminishes within three laminate thicknesses from the crack tip and is independent of delamination length. Therefore, a single finite element model in conjunction with the flexural analysis is sufficient to characterize the stress state in the vicinity of the crack tip. The interlaminar normal stress distribution at the crack tip corresponds to a crack closing moment which significantly influences strength predictions. The analytical approach for the prediction of compressive strength consists of the strain-energy release

rate for a cantilever beam loaded by a moment where the total moment has contribution from both the opening and closing moments. A value of G_{IC} = 1.4 lb/in (250N/m) provides excellent correlation of experimental data with analytic predictions of the compressive strength for the delamination geometries investigated.

REFERENCES

1. Ashizawa, M., "Fast Interlaminar Fracture of a Compressively Loaded Composite Containing a Defect," Fifth DoD/NASA Conference on Fibrous Composites in Structural Design, 1981.

2. Gillespie, J. W. and Pipes, R. B., "Compression Strength of Composite Materials with Interlaminar Defects," Center for Composite Materials Report CCM79-17, 1979.

3. Whitcomb, J. D., "Finite Element Analysis of Instability Related Delamination Growth," Journal of Composite Materials, Vol. 14, 1981, p. 403.

4. Chai, Hazl, "The Growth of Impact Damage in Compressively Loaded Laminates, " Ph.D. Dissertation, California Institute of Technology, 1982.

5. Whitcomb, J. D., "Approximate Analysis of Postbuckled Through-Width Delaminations," NASA Technical Memorandum 83147, 1981.

6. Pipes, R. B. and Pagano, W. J., "Interlaminar Stresses in Composite Laminates - An Approximate Elasticity Solution," Journal of Applied Mechanics, Vol. 41, 1974, p. 668.

7. Lawn, B. R. and Wilshaw, T. R., Fracture of Brittle Solids, Cambridge University Press, Cambridge, 1975, p. 62.